Remote Sensing of Environment 240 (2020) 111669

Contents lists available at ScienceDirect

Remote Sensing of Environment

journal homepage: www.elsevier.com/locate/rse

Integrating airborne laser scanning data, space-borne radar data and digital aerial imagery to estimate aboveground carbon stock in Hyrcanian forests, Iran

Maryam Poorazimy[a,*], Shaban Shataee[a], Ronald E. McRoberts[b,c], Jahangir Mohammadi[a]

[a] Department of Forestry, Gorgan University of Agricultural Sciences & Natural Resources, Gorgan, Iran
[b] Northern Research Station, U.S. Forest Service, Saint Paul, MN, USA
[c] Department of Forest Resources, University of Minnesota, Saint Paul, MN, USA

ARTICLE INFO

Keywords:
REDD
ALS
Radar
UltraCam
Model-assisted estimators
Relative efficiency

ABSTRACT

A framework for estimating aboveground forest carbon stock (AFCS) is required for measurement, reporting, and verification (MRV) systems under the United Nations Collaborative Program on Reducing Emissions from Deforestation and Forest Degradation (REDD) in Developing Countries. Recently, methods for estimating the spatial distribution of AFCS using remotely sensed datasets and multiple prediction techniques have been found to be useful, particularly given the prohibitive costs of acquiring the necessary sample sizes for sufficiently precise pure field-based estimation of this variable. The objective of the study was to assess and compare the capabilities of airborne laser scanning (ALS) data, L-band radar data and UltraCam images in combination with four commonly used prediction techniques for estimating mean AFCS per unit area: multiple linear regression (MLR) and the nonparametric k-Nearest Neighbors (k-NN), support vector regression (SVR), and random forest (RF) algorithms. Our study area was a part of Hyrcanian deciduous forests in two managed and unmanaged stands at Shast Kalateh forest. We used a systematic sample consisting of 308 circular field plots of 0.1 ha located at the intersections of a 150 × 200 m grid with a random starting point and remote sensing-derived metrics as auxiliary data. We used 67% of the sample plots for training purposes and the remaining 33% for validation. Also, we used the model-assisted estimators to statistically rigorously estimate mean AFCS per unit area and its standard error (SE).

Among the remotely sensed datasets, considered singly, the ALS data with $R^{2*} = 0.34$, rRMSE = 47.42% and relative efficiency (RE) = 1.51 produced the greatest accuracy and precision for AFCS estimation. RE can be interpreted as the factor by which the sample size for the pure field-based estimator would have to be increased to obtain the same precision as for the model-assisted estimator using auxiliary data. Among the remotely sensed datasets considered in combination, the ALS and PALSAR dataset with $R^{2*} = 0.41$, rRMSE = 44.80% and RE = 1.70 produced the greatest prediction accuracy and precision and increased the proportion of variability explained relative to ALS and PALSAR separately by 7% and 36%, respectively. Contrary to our expectation, the combination of PALSAR and UltraCam data decreased the precision of AFCS estimates. All the remotely sensed datasets, singly and in combination, with the most accurate prediction techniques for each combination produced estimates of AFCS that were within the 95% confidence interval for the field-based estimate.

1. Introduction

1.1. Background and motivation

Forest ecosystems contain 80% of the terrestrial carbon stock in the aboveground biomass pool and 40% of the terrestrial carbon stock in the roots, litter and organic soils pools (Wani et al., 2015; García et al., 2010). Changes in cover, use and management of forests can affect the transfer of carbon dioxide between terrestrial ecosystems and the biosphere (Vashum and Jayakumar, 2012; García et al., 2010; Brown et al., 1989). Thus, forests play a key role in the global carbon cycle, and forest monitoring is an important component of programs such as REDD + (Reducing Emission from Deforestation and forest Degradation, plus the sustainable management of forests, and the conservation and

* Corresponding author.
E-mail address: m.poorazimy@gau.ac.ir (M. Poorazimy).

https://doi.org/10.1016/j.rse.2020.111669
Received 10 May 2019; Received in revised form 24 December 2019; Accepted 16 January 2020
Available online 06 March 2020
0034-4257/

enhancement of forest carbon stocks) and GOFC-GOLD (Global Observation of Forest and Land Cover Dynamics) (Hopkinson et al., 2016; Carreiras et al., 2012; Tsui et al., 2012; García et al., 2010). Aboveground, living tree biomass (AGB) is the largest forest carbon pool that is directly influenced by deforestation and forest degradation (Vashum and Jayakumar, 2012; Gibbs et al., 2007). The carbon concentrations of different tree parts generally vary between 47% and 53% of tree biomass, depending on species (Vashum and Jayakumar, 2012; García et al., 2010), and in the absence of local information are commonly assumed to be approximately 50% (Wani et al., 2015; Galeaña-Pizaña et al., 2014; García et al., 2010; Houghton, 2005). Accordingly, prediction of tree biomass is recognized as an important step in estimation of aboveground forest carbon stock (AFCS).

Once allometric models are selected or constructed, field plot measurements are traditionally used to predict individual tree biomass. However, these models have disadvantages and are often difficult to obtain, especially for remote areas. Also, they do not provide the spatial distribution of biomass at large scales, especially in many developing countries such as Iran which have no well-established national forest inventory (NFI) or monitoring system. A complementary approach is to augment field data with remotely sensed auxiliary datasets that provide spatially continuous and temporally explicit information for large areas. Hence, estimation of biomass carbon stock using auxiliary data from airborne and space-borne remote sensing sources has emerged in recent decades (Thapa et al., 2015; Asner and Mascaro, 2014; Lu, 2006). Nevertheless, field data are still necessary for calibration and validation of remote sensing-assisted prediction techniques. Although considerable research has addressed estimation of biomass carbon stock using optical, radar and airborne laser scanning (ALS) data, singly or in combination, with both parametric and nonparametric techniques, accurate biomass carbon stock estimation is still challenging.

1.2. Remotely sensed datasets

ALS sensors are a source of remotely sensed auxiliary data that can produce height information which, in turn, can be used to assist in constructing accurate maps of forest attributes such as biomass and enhancing inferences for population parameters (Chen et al., 2016; Asner and Mascaro, 2014; Zolkos et al., 2013; Kronseder et al., 2012; Latifi et al., 2012; Tian et al., 2012). However, their cost and limited availability inhibits widespread application for forest assessments (Lu et al., 2014; Vaglio Laurin et al., 2014; Zald et al., 2016). The capabilities of space-borne synthetic aperture radar (SAR) systems to acquire cloud-free and wall-to-wall images make them useful instruments for tracking forest carbon. Long wave SAR systems with their canopy penetration capability can contribute to the volumetric analysis that is required for biomass carbon stock estimation. (Thapa et al., 2015; Sinha et al., 2015; Tsui et al., 2013; Tian et al., 2012; Saatchi et al., 2011). However, signal saturation is a problem for biomass carbon stock prediction via a direct approach using radar responses (e.g., backscatter, SAR coherence), thereby limiting SAR capability for prediction of large density biomass (Imhoff, 1995; Dobson et al., 1992). Optical sensors are a common source of auxiliary data for biomass carbon stock prediction with many studies using medium spatial resolution data (Fernández-Manso et al., 2014; Wani et al., 2015; Yadav and Nandy, 2015). However, optical remotely sensed data have limited capability for predicting forest vertical structure, and when crown closure is reached, differences in spectral responses diminish with the result that prediction tends to become asymptotic (Lu et al., 2014; Tsui et al., 2012). In addition to less biophysically complex areas, increases in spatial, radiometric and temporal resolution associated with aerial imagery generally improve biomass carbon stock prediction. Aerial imagery can be a source of high quality, wall-to-wall, remotely sensed data for estimating forest biomass on small- to medium-sized forests, or as a sampling tool in large forest areas, with relatively small costs (Kachamba et al., 2016). Despite the individual drawbacks of these remotely sensed data, many studies have demonstrated that integration of data from multiple remote sensors can increase the precision of biomass carbon stock estimates (Vaglio Laurin et al., 2014; Anderson et al., 2008; Tsui et al., 2012; Zhao et al., 2016).

1.3. Prediction techniques and statistical inference

Multiple prediction techniques, each based on different underlying assumptions and complexity, can be used to predict biomass carbon stock. Many studies have demonstrated that regression models using remotely sensed auxiliary data are effective for predicting biomass carbon stock, but the results may be poor in the cases of insufficient ground sample sizes and/or weak regression-based relationships between biomass carbon stock and predictor variables (Lu et al., 2014). Non-parametric algorithms, some of which use machine learning, are alternative approaches.

Although prediction accuracy for sample units is of particular interest, it is coming to be recognized as only an intermediate step enroute to an inference in the form of a confidence interval for population parameters such as the mean and its standard error (SE) (McRoberts et al., 2016). Models are increasingly used in large area forest surveys because of improved availability of remotely sensed auxiliary data (Ståhl et al., 2016). Model-assisted regression estimators which rely on probability samples for validity can increase the precision of estimates and, thereby, enhance inferences (Särndal et al., 1992). Relative efficiency (RE) can be used to assess the contribution of remotely sensed datasets for improving the precision of AFCS estimates beyond that obtained for pure field-based estimates and to assess the relative cost of increasing ground sample sizes versus the cost of acquiring remotely sensed auxiliary data and constructing maps (GFOI, 2016).

1.4. Objectives

Biomass carbon stock estimation is of growing interest in Iran, with only a few studies having been conducted using optical data. Further, ALS data have not been used for biomass carbon stock prediction in Iran, and the capability of radar data is not completely understood. Therefore, our research focused on estimating AFCS in Hyrcanian forests of Iran with three specific objectives: (i) to evaluate the capability of ALS data, L-band radar data and aerial digital images, singly and in combination, (ii) to compare the multiple linear regression (MLR), k-Nearest Neighbors (k-NN), support vector regression (SVR), and random forest (RF) prediction techniques, and (iii) to construct statistical inferences using the model-assisted estimator and quantify the precision gain in AFCS estimates for different remotely sensed datasets.

2. Materials and methods

2.1. Site description

The study was conducted in Shast Kalateh forest which is managed by the Gorgan Forestry College and is located in northern Iran on the shores of the Caspian Sea (Fig. 1). This forest is a part of Hyrcanian forests which are remnants of the Pleistocene period (Sagheb-Talebi et al., 2014). The study area is bounded by 54°21′-54°24′ E and 36°44′-36°46′ N and includes 1100 ha of logged managed and unmanaged temperate deciduous forests. The dominant aspect is western, and elevation ranges from 270 to 740 m above sea level. Based on the Amberejeh climate classification, the study area is characterized as middle humid climate with mean annual precipitation of 649 mm and mean annual temperature of 15.4 °C. *Parrotia persica*, *Carpinus betulus*, *Fagus orientalis* and *Diospyros lotus* are the dominant tree species.

2.2. Field-based AFCS estimation

We used field data for 308 circular sample plots of 0.1 ha

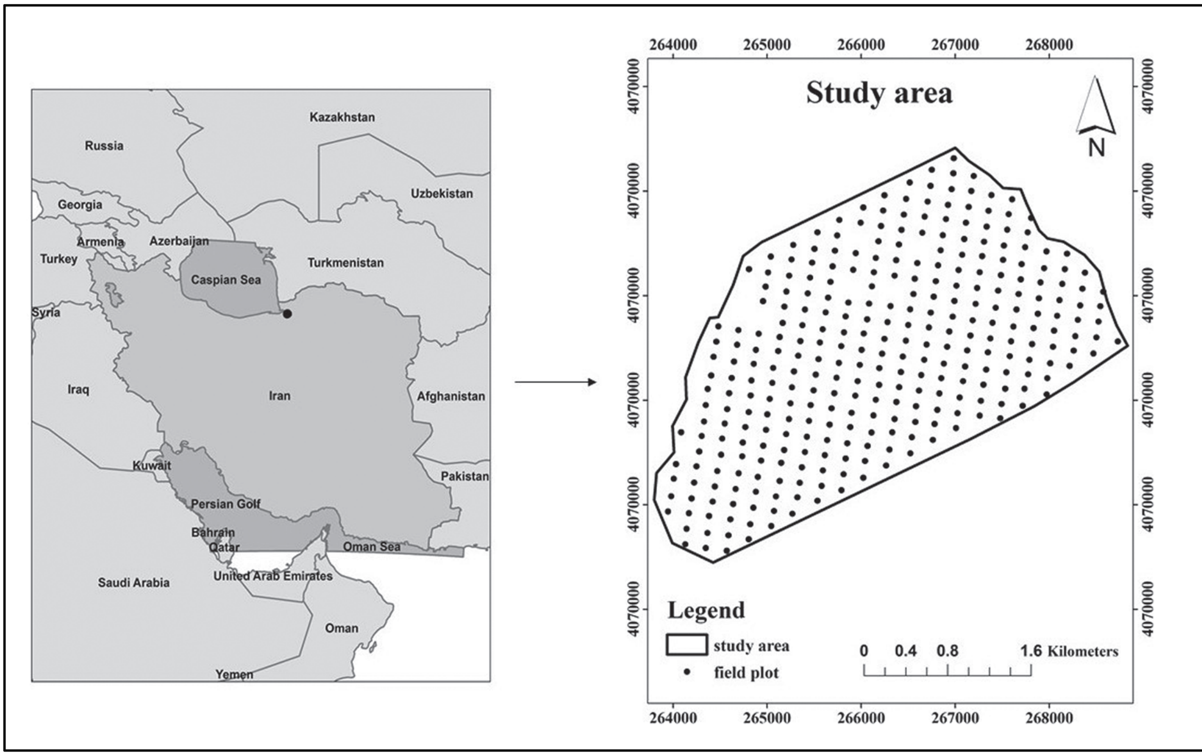

Fig. 1. Study area in Iran, Shast Kalateh forest.

Table 1
Summary of plot biophysical properties.

Variable	Min	Max	Mean	Std dev.
Mean dbh (cm)	18.05	67.18	34.48	8.24
Mean height (m)	7.13	28.70	19.99	2.92
Volume (m^3)	0.45	71.71	26.28	11.60

(radius = 17.84 m) that were measured in 2011. The plots were located at the intersections of a 150 × 200 m grid with a random starting point. Plot center coordinates were estimated by means of differential global positioning system (DGPS). For each tree with diameter at breast height (dbh) of at least 12.5 cm, tree species, dbh measured with a caliper and height measured with a Vertex (VL402) were recorded (Mohammadi, 2013) (Table 1).

For predicting individual tree AGB, we used species-specific allometric models developed for Shast Kalateh forest using tree size properties as predictor variables (Shamsi Jamkhaneh, 2012). These species-specific allometric models were used to predict tree AGB for the main tree species, and a general model based on the main species data was used for other relatively rare species. For this study, the uncertainty associated with the allometric model predictions was considered negligible and ignored.

Plot-level AGB was converted to carbon content via multiplication by a standard conversion factor of 0.48 for temperate and boreal broad-leaved forests (IPCC, 2006). A variogram analysis indicated no meaningful spatial correlation among plot-level AFCS data which contributes to the efficiency of the inventory sampling. Minimum, maximum and mean plot-level AFCS were 3.95, 218.78, and 53.02 Mg ha^{-1}, respectively, with standard deviation of 32.35 Mg ha^{-1}. A range of structural stages from regeneration stands with small AFCS to mature stands with large AFCS revealed biophysically complex conditions on the study site.

2.3. *Remotely sensed data*

2.3.1. *Airborne laser scanning data*

ALS data were acquired on 12 October 2011 under leaf-on canopy conditions using a Riegl LMS Q560 laser scanner (1064 nm wavelength) mounted on a TB-20 aircraft at a mean flying altitude of 1000 m above sea level. The sensor has a maximum pulse repetition frequency of 240 kHz with scan angle range of 22.5°–30°, resulting in average pulse density of 4 pulses m^{-2} on the ground. The ALS data were processed by the Rayan Naghsheh Company. All returns were classified as first returns, last returns and other returns using RoiProcess software, and outliers were delineated in TerraScan software. Ground points were removed using the Kraus and Pfeifer (1998) algorithm and a digital terrain model (DTM) was constructed using the triangulated irregular network (TIN) interpolation method with 1-m pixel size. The mean elevation difference between the DTM and 90 ground control points showed mean DTM accuracy of 40 cm. A 2-m minimum height was used to distinguish shrubs and understory vegetation returns from returns for relevant parts of trees.

Canopy height and density metrics. Canopy height metrics including height percentiles (1st, 5th, 10th, …, 99th) and other standard height metrics such as the mean and coefficient of variation were calculated (Næsset, 2004; Lim and Treitz, 2004; Patenaude et al., 2004). Further, we derived canopy density metrics that represented the relative cumulative frequencies of returns from the top of the canopy to the 2-m threshold height at different height levels in the canopy (Næsset et al., 2016; Gregoire et al., 2016). In addition, amplitudes and canopy closure (the ratio of returns at the given height to all returns) were calculated using the Fusion software (McGaughey, 2015). The ALS metrics for first and last returns were calculated separately for 31.62 × 31.62-m pixels that corresponded to the plot size.

2.3.2. *Radar data*

Fine Beam Dual (FBD) scenes in both horizontal transmit/horizontal receive (HH) and horizontal transmit/vertical receive (HV) polarization channels by the Phased Array L-band Synthetic Aperture Radar (PALSAR) instrument on the Advanced Land Observation Satellite (ALOS) were acquired for 7 July 2009. The scene was delivered in single look complex (SLC) format with incidence angle of approximately 38°. To enhance the radiometric resolution and to achieve approximately square pixels, the radar data were multi-looked using factors of 1 and 5 for range and azimuth direction. A 10-m DEM retrieved from topographic maps was used to terrain-correct geocoding and lastly, all of the images were geocoded to the previously mentioned pixel size.

Backscattering coefficient and rational variables. The backscattering coefficient measures the intensity of energy per unit area that is dispersed by an object (Galeana-Pizaña et al., 2014). As per Eq. (1), image intensity can be converted to a backscatter coefficient in the form of σ^0 (Shimada et al., 2009):

$$\sigma^\circ = \sigma\frac{A_{flat}}{A_{slope}}, \tag{1}$$

where σ is the uncorrected backscattering coefficient which depends on the system's pixel size, A_{flat} is SAR pixel size for flat terrain, and A_{slope} is true local SAR pixel size. Previous studies have reported that sloped terrain can induce 2–7 dB dispersion on radar backscatter (Castel et al., 2001), a non-negligible problem when assessing backscatter properties. The Kellndorfer et al. (1998) normalization method with respect to the dependence of surface and volume scattering on the local incidence angle can be used to address these topographic effects. Using Eq. (2) (Santoro et al., 2006), we converted σ^0 to γ^0 backscattering coefficient (Attarchi and Gloaguen, 2014; Carreiras et al., 2012; Ulander, 1996):

$$\gamma^\circ = \sigma^\circ\left(\frac{\cos(\theta_{iref})}{\cos(\theta_{iloc})}\right)^m, \tag{2}$$

where θ_{iref} is the incidence angle at a reference location (e.g., mid-swath), θ_{iloc} is the local incidence angle, and m is the optical canopy depth as a site-specific factor ranging between 0 and 1, but because it is difficult to measure, it is commonly assumed to be 1 (Kim, 2012; Lucas et al., 2010; Santoro et al., 2009; Thiel et al., 2009). We also calculated the ratio of HH and HV (HH/HV) and the difference between HH and HV (HH–HV) (Jinwei et al., 2012), both of which have been used for forest and forest change monitoring (Miettinen and Liew, 2011; Wu et al., 2011).

Textural and polarimetry measures. As additional predictors of forest structure, the Gray Level Co-occurrence Matrix (GLCM) was calculated (Haralick et al., 1973). The GLCM controlling parameters were window sizes of 3 × 3, 5 × 5, 7 × 7, 9 × 9 and 11 × 11 pixels with a horizontal and vertical shift of 1.0 for each of the γ^0 backscattering coefficients separately. We extracted textural metrics including mean, variance, correlation, homogeneity, contrast, dissimilarity, entropy, and second moment with the best window of 11 × 11. The Cloude and Pottier (1997) target decomposition was applied for the PALSAR data, an enhanced Lee filter with a window size of 5 × 5 pixels was used (Lee, 1981), and performance was evaluated. Accordingly, the alpha angle (α) and entropy (H) were computed to characterize the interactions of the feature's physical properties with its polarimetric behavior.

2.3.3. Digital areal imagery

Aerial images were acquired using Vexel UltraCam-D on 12 October 2011, contemporary with the ALS data. This imagery contains five bands: panchromatic, blue, green, red, and near-infrared. Resolution of the CCD-based sensor (Charge Couple Device) was 11,500 × 7500 pixels in panchromatic and 4008 × 2672 pixels in multispectral bands. The sensor flight altitude of 1000 m above sea level with a focal length of 101.04 mm for the panchromatic band resulted in a resampled ground pixel size of 15 cm. These pan-sharpened images were prepared by the Rayan Naghsheh Company to correction level 2. For greater geometric calibration, we used the ALS DTM which resulted in an RMSE of 1.2 pixels. In addition to the five bands with the radiometric depth of 16 bit, we used artificial color composite infrared (CIR) band in our analyses.

Table 2
Vegetation indices.

Index	Formulation	Reference
SRI	$\frac{Nir}{Red}$	Birth and McVey (1968)
NDVI	$\frac{Nir - Red}{Nir + Red}$	Rouse et al. (1973)
DVI	$Nir - Red$	Tucker (1979)
SAVI	$\frac{Nir - Red\ (1 + 0.5)}{Nir + Red + 0.5}$	Huete (1988)
RDVI	$\sqrt{NDVI \times DVI}$	Roujean and Breon (1995)
VIS123	$Blue + Green + Red$	Lu et al. (2004)
GNDVI	$\frac{Nir - Green}{Nir + Green}$	Buschmann and Nagel (1993)
ND32	$\frac{Red - Green}{Red + Green}$	Mathieu et al. (1998)
ARVI	$\frac{Nir - 2Red + Blue}{Nir + 2Red - Blue}$	Kaufman and Tanre (1992)

Vegetation index and textural measures. Many vegetation indices that reduce the effects of shadows and environmental conditions on reflectance values have been proposed to enhance biomass prediction in complex forest structures (Lu, 2006). We examined nine such indices (Table 2). Further, we calculated 13 textural metrics including contrast and its gray level difference vector (GLDV), mean and its GLDV, entropy and its GLDV, angular second moment and its GLDV, correlation, variance, dissimilarity, homogeneity, and inverse difference for each spectral band. An optimal window size of 150 × 150 pixels was used for calculating textural metrics (Mohammadi, 2013).

2.4. Prediction techniques

2.4.1. Multiple linear regression

An MLR model with stepwise selection of predictor variables was used to predict the relationship between log-transformed AFCS and metrics derived from the remotely sensed datasets, singly and in combination. To abate overfitting problems caused by the large number of independent variables, we used only predictor variables with large importance as estimated from the RF algorithm (Section 2.4.2). Collinearity in the selected model variables was investigated using the variance inflation factor (VIF) (Belsley et al., 1980). We used residuals analysis to assess and improve the fit of the MLR models to our data. We corrected for the bias that occurs when back-transforming from the logarithmic to the original AFCS scale (Baskerville, 1971).

2.4.2. Nonparametric algorithms

k-NN is a widely used prediction technique for use with combinations of forest inventory and remotely sensed data (Chirici et al., 2016; McRoberts, 2012; Tomppo et al., 2008; Zhou et al., 2011). The set of sample units for which response and predictor variables are available is designated the reference set, and the set of population units for which response variable predictions are required is designated the target set (McRoberts et al., 2015). For the number, k, of nearest or similar reference units (neighbors), we considered values ranging from 1 to 50. For the ith target unit, the k-NN prediction is (Eq. (3)):

$$\hat{y}_i = \sum_{j=1}^{k} w_{ij} y_j^i, \tag{3}$$

where, the subscript j indexes the selected nearest neighbors which are equally weighted ($w_{ij} = 1/k$). We compared Euclidean, Squared Euclidean, Manhattan and Chebyshev distance metrics (Gjertsen, 2007). We used the leave-one-out (LOO) cross validation technique to optimize the k-NN algorithm.

SVR has been shown to reduce overfitting, although use of SVR for biomass prediction is not common (Marabel and Alvarez-Taboada, 2013). SVR assumes that each set of predictor variables has a unique relationship with the response variable, and that the groupings and relationships among these predictors are sufficient to formulate rules that can be used for future prediction. HyperPlanes accomplish this task in a multi-dimensional feature space built from axes representing the predictor variables (Gleason and Im, 2012). Also, SVRs can overcome linear regression limitations by using kernels (Lu et al., 2014). Therefore, we examined linear, polynomial (degree 2 and 3), radial base function and sigmoid kernels in this study. Grid search SVR parameter optimization, a classic approach that relies on gradient descent convergence (Gleason and Im, 2012), was used to select SVR parameter values.

RF uses regression trees to estimate the relationship between response and predictor variables and is widely used for biomass prediction (Tanase et al., 2014; Hudak et al., 2012). Decision trees continue to grow until the minimum error relative to the response variable is obtained. RF models have been shown to reduce overfitting and systematic errors (Breiman, 2001), and in some cases have produced greater accuracies than linear regression models for biomass prediction (Powell et al., 2010). For all regression trees within an RF implementation, the optimal number of predictor variables was selected from within the range $\sqrt{number\ of\ predictor\ variables} \pm 2$.

2.5. Statistical analyses

2.5.1. Accuracy assessment

We randomly divided the sample data S into training and validation subsets, denoted S_{trn} and S_{val} respectively; trained the prediction algorithms using the S_{trn} dataset; and assessed accuracy using the S_{val} dataset. Accordingly, the distributions of the sample plot data in the S_{trn} and S_{val} datasets becomes important. We sorted the plots with respect to AFCS values from minimum to maximum and then selected every third plot for the S_{val} dataset with the result that the S_{trn} dataset included 206 plots and the S_{val} dataset included 102 plots. The result was that our S_{trn} and S_{val} datasets had comparable distributions over the study area. All models were evaluated using relative root mean square error (rRMSE) and relative mean deviation (rMD) (Eqs. (4) and (5)):

$$rRMSE = \frac{\sqrt{\sum_{i \in S_{val}} \frac{(\hat{y}_i - y_i)^2}{n}}}{\bar{y}} \times 100, \tag{4}$$

$$rMD = \frac{\sqrt{\sum_{i \in S_{val}} (\hat{y}_i - y_i)/n}}{\bar{y}} \times 100, \tag{5}$$

where $\hat{y}_i$ is the predicted value, y_i is the observed value, $\bar{y}$ is the mean, n is the S_{val} sample size, and i indexes the elements of S_{val}. In addition, pseudo-R^2 (R^{2*}) was calculated as:

$$R^{2*} = \frac{SS_{mean} - SS_{res}}{SS_{mean}}, \tag{6}$$

where

$$SS_{mean} = \sum_{i \in S_{val}} (y_i - \bar{y})^2$$

and

$$\bar{y} = \frac{1}{n} \sum_{i \in S_{val}} y_i.$$

The analyses consisted of optimizing each of the MLR, k-NN, SVR and RF algorithms for each of the remotely sensed auxiliary datasets. For each remotely sensed dataset. The algorithm that produced the greatest accuracy was used to estimate the population mean and its SE (Section 2.5.2).

2.5.2. Population parameter estimation

For inventory purposes, an important objective is an inference in the form of a confidence interval for a population parameter expressed in terms of the estimated mean and its SE. Because our 308 sample plots comprised an equal probability sample of the population, we adopted the asymptotically unbiased, model-assisted estimators that rely on probability samples for validity (McRoberts et al., 2015; Särndal et al., 1992, Section 6.5):

$$\hat{\mu}_{MA} = \frac{1}{N} \sum_{i \in U} \hat{y}_i - \frac{1}{n} \sum_{i \in S_{val}} (\hat{y}_i - y_i) \tag{7}$$

and

$$v\hat{a}r(\hat{\mu}_{MA}) = \frac{1}{n(n-1)} \sum_{i \in S_{val}} (\hat{y}_i - y_i)^2, \tag{8}$$

where U denotes the population and N is the population size.

An important aspect of this study was comparing the contribution of each remotely sensed dataset for improving AFCS estimation beyond pure field-based estimation. A common measure of this contribution is relative efficiency (RE) (Eq. (9)):

$$RE = \frac{v\hat{a}r(\hat{\mu}_{Field})}{v\hat{a}r(\hat{\mu}_{MA})}, \tag{9}$$

where $v\hat{a}r(\hat{\mu}_{MA})$ as expressed by Eq. (8) is the model-assisted variance estimator for a particular remotely sensed dataset and $v\hat{a}r(\hat{\mu}_{Field})$ as expressed by Eq. (10) is the variance estimator for a simple random or systematic sampling design:

$$v\hat{a}r(\hat{\mu}_{Field}) = \frac{\sum_{i \in S_{val}} (y_i - \hat{\mu}_{Field})^2}{n(n-1)} \tag{10}$$

where

$$\hat{\mu}_{Field} = \frac{\sum_{i \in S_{val}} y_i}{n}.$$

RE can be interpreted as the factor by which the sample size for the pure field-based estimators of Eq. (10) would have to be increased to obtain the same precision as for the model-assisted estimator using auxiliary data. Athough the variance estimator of Eq. (10) is slightly biased when used with systematic samples, the bias is conservative in the sense that it produces an overestimation and, therefore, was ignored for this study (Särndal et al., 1992).

3. Results and discussion

3.1. Remotely sensed datasets

3.1.1. ALS data

ALS-derived canopy height metrics are strongly correlated with even large biomass (>1000 Mg ha^{-1}) (e.g., Means et al., 1999), and they can circumvent the accuracy problems associated with using optical and radar data for predicting biomass. The k-NN prediction technique was the most accurate for the ALS remotely sensed dataset, explaining 34% of the variation in the AFCS observations with rRMSE = 47.42% (Table 3-A). These fit statistics indicate somewhat less accuracy than reported for some other studies, but are comparable to those reported for Central Kalimantan using full waveform ALS with rRMSE = 33.85% in both lowland dipterocarp and peat swamp rain forest types (Kronseder et al., 2012). Also, Næsset et al. (2016) reported rRMSE = 55.6% for AGB estimation in southeastern Tanzania. Our somewhat smaller accuracies can possibly be attributed to several factors. First, smaller trees with dbh < 12.5 cm were not measured in the

Table 3-A
Most accurate AFCS models using single remotely sensed datasets.

Dataset (singly)	Algorithm	Pseudo R^2 (R^{2*})	rMD (%)	RMSE (Mg ha^{-1})	rRMSE (%)
ALS	MLR	0.26	−6.14	26.34	50.07
	k-NN	0.34	−4.32	24.95	47.42
	SVR	0.31	−7.85	25.36	48.21
	RF	0.30	−2.48	25.65	48.77
PALSAR	MLR	−0.04	−12.95	31.29	59.49
	k-NN	0.04	0.92	30.02	57.06
	SVR	−0.37	26.86	36.08	68.58
	RF	0.05	−0.11	29.93	56.89
UltraCam	MLR	0.24	−6.41	26.75	50.85
	k-NN	0.18	−0.31	27.70	52.65
	SVR	0.20	2.60	27.42	52.12
	RF	0.21	−0.06	27.19	51.69

field, but were still represented in the ALS return heights. Second, our 0.1-ha plots were considerably larger than the 0.05-ha plots commonly used for boreal and temperate inventories (Tomppo et al., 2008), but were smaller than the 0.5-ha plots used for tropical forests to reduce among-plot variances, boundary effects due to large crowns (Mascaro et al., 2011) and the effects of GPS positional errors (Mauya et al., 2015). Third, although we have infrequent mismatches between field plot locations and corresponding areas for which ALS height metrics were calculated, these mismatches likely caused adverse boundary effects. Gleason and Im (2012) reported rRMSE = 13.6% for biomass predictions which can be attributed to little variation among the forest properties, large plots with radius of 11 m, and an ALS system with a large pulse density of 12.7 pulses m^{-2}. However, García et al. (2010) showed that the reduction of ALS pulse density had only a small effect on AGB prediction accuracy for general models with all species and decreased R^2 from 0.70 for 1.5–4.5 pulses m^{-2} to 0.60 for 0.97–2.1 pulses m^{-2}.

3.1.2. PALSAR data

For use with the PALSAR dataset, the RF algorithm with rRMSE = 56.89% was more accurate than the other algorithms (Table 3-A). However, the small R^{2*} = 0.05 signified no meaningful relationship between AFCS and the radar metrics. This weak result can be at least partially attributed to the complex site conditions relative to the spatial and vertical forest structures that lead to signal saturation. Other specific site conditions such as soil surface roughness and soil moisture are also related to signal saturation (Hamdan et al., 2015; Lu et al., 2014; Suzuki et al., 2013; Koch, 2010; Austin et al., 2003). From Fig. 2, it can be seen that the AFCS saturation limit for this study was approximately 50 Mg ha^{-1} (Imhoff, 1995; Luckman et al., 1997; Le Toan et al., 2004) suggesting that the PALSAR data may not be sensitive to our large AFCS range. Within-plot species diversity, topography, and tree-to-tree variability in the study area are other factors that contribute to this weak result. Zhao et al. (2016) reported relatively inaccurate AGB prediction with R^2 = 0.19 and rRMSE = 37.4% using PALSAR textural information from the HH and HV channels (without selecting the best window size). In the mixed forests of eastern China, Tsui et al. (2012) reported that the L-band HV coherence with adjusted R^2 = 0.47 did not appear to be more sensitive than L-band HV backscatter with adjusted R^2 = 0.61. However, in the latter study, L-band HH backscatter was not significantly correlated with AGB. Similarly, Næsset et al. (2016) reported that mean height of InSAR from TanDEM-X as an explanatory variable yielded rRMSE = 78.6% and R^2 = 0.25, contrary to reports of most other studies. Many studies have reported the influence of plot size on the strength of relationships between AGB/AFCS and radar data. As an example, larger plots (Saatchi et al., 2011; Carreiras et al., 2012) or with a difference in size (Mitchard et al., 2009) improved prediction, especially in stands with greater species diversity. Thapa et al. (2015) achieved RMSE = 28 Mg ha^{-1} for AFCS prediction using PALSAR mosaic textural metrics, and backsctter coefficients with their ratios from 2009 and 2010 in central Sumatra. Except for the biophysically complex conditions in their study area and 25 m resolution of PALSAR mosaic data, they used two temporal radar datasets with a plot size of 1.0 ha that can affect their results. In mountain Hyrcanian forests using polarimetric and textural metrics of dual PALSAR data, Attarchi and Gloaguen (2014) reported rRMSE = 21.90% and adjusted R^2 = 0.45. This result may be attributed to a homogenous site condition resulting from shelterwood cutting and a plot size of 0.36 ha. The DEM used may have contributed to some of the error in our study by not completely eliminating the significant topographic influence. As shown by Attarchi and Gloaguen (2014), precise slope correction can improve textural quality and AGB prediction. The proportion of variability explained in our study is within the range of reports for other studies (Vafaei et al., 2018; Stelmaszczuk-Górska et al., 2018; Pereira et al., 2018; Pham et al., 2018; Omar et al., 2017; Zhao et al., 2016; Deng et al., 2014).

3.1.3. UltraCam data

MLR was the most accurate prediction technique for use with UltraCam data with rRMSE = 50.85% and R^{2*} = 0.24. Ronoud (2016) reported rRMSE = 14.3% for AGB prediction using Landsat-8 data in a pure Hyrcanian forest, and Fernández-Manso et al. (2014) reported rRMSE = 37.7% for AGB estimation in managed pine woodlands using ASTER fraction image and linear spectral mixture analysis (LSMA). In another study in a mixed Hyrcanian forest with SPOT-HRG data, Fathollahi (2013) reported rRMSE = 42.77%. With respect to the greater spatial and radiometric resolution of the UltraCam data relative to the other remotely sensed data, this result was not as expected. Using Quickbird data for the same study area, Mosavi (2015) reported rRMSE = 60.48% which was less than our result. Galeaña-Pizaña et al. (2014) used SPOT-HRG NDVI variable for pine forests and SAVI variable for fir forests with regression-kriging and achieved RMSE = 33.49 and RMSE = 45.43 Mg ha^{-1} for AFCS prediction, respectively.

3.1.4. Combinations of remotely sensed data

Table 3-B shows the performance of the prediction techniques using combinations of remotely sensed datasets. The combined ALS and PALSAR dataset using the k-NN algorithm produced the greatest accuracy with R^{2*} = 0.41 and rRMSE = 44.80%. This combination increased the proportion of variability explained by 7% and 36%, respectively, relative to ALS and PALSAR datasets separately. Tsui et al. (2012) reported that the addition of entropy and the backscattering coefficient of C-band radar to the most accurate ALS-based model reduced AGB prediction error to 8% which is comparable to our results. Also, the combination of ALS and UltraCam produced greater accuracy, rRMSE = 45.49%, than using either of them separately. Similarly, Vaglio Laurin et al. (2014) reported improved accuracy of AGB prediction to RMSE = 61.7 Mg ha^{-1} and adjusted R^2 = 0.70 using a combination of ALS and hyperspectral imagery in an African tropical forest. The addition of PALSAR metrics to UltraCam metrics resulted in a 0.33% precision decrease relative to using UltraCam separately. The combination of ALS, PALSAR and UltraCam produced no improvement in accuracy relative to the most accurate dataset combination. Contrarily, for a study in a Hyrcanian forest, Amini and Sadeghi (2011) showed that the integration of optical and dual radar data from the ALOS satellite improved RMSE to 13.88 Mg ha^{-1} for AGB prediction. Attarchi and Gloaguen (2014) reported for mountain Hyrcanian forests that combining PALSAR-derived metrics and TM data improved the error of prediction to 12.68%. Although, Tian et al. (2012) reported a slight decrease in the accuracy of AGB prediction when HV backscatter of PALSAR was added to most significant Principle Component Analysis (PCA) of SPOT-HRG and auxilary variables of Infrared Index (IRI) and DEM.

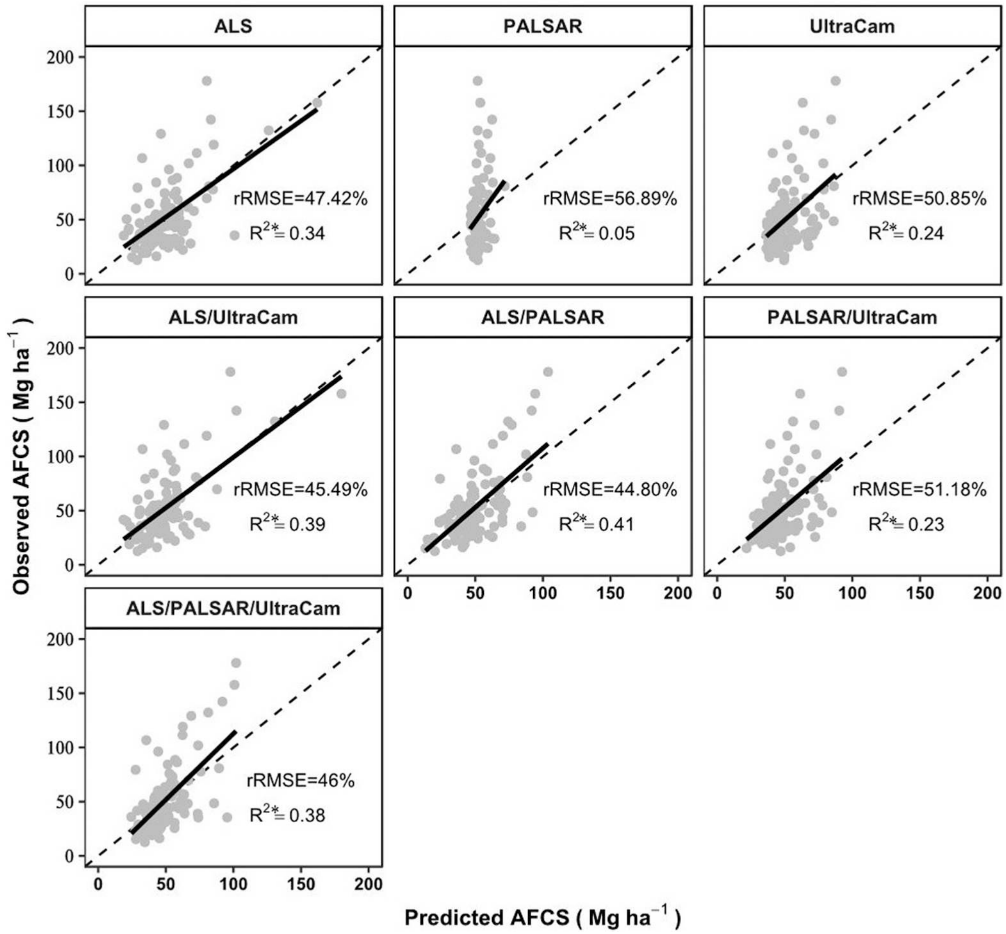

Fig. 2. Observed versus predicted AFCS for the 102 validation plots with the dashed line representing the 1:1 relationship and solid line representing fitted linear regression model.

Table 3-B
Most accurate AFCS models using combinations of remotely sensed datasets.

Dataset (in combination)	Algorithm	Pseudo R^2 (R^{2*})	rMD (%)	RMSE (Mg ha^{-1})	rRMSE (%)
ALS/PALSAR	MLR	0.28	−6.26	25.94	49.31
	k-NN	0.41	−5.03	23.57	44.80
	SVR	0.32	−5.30	25.34	48.17
	RF	0.29	−2.85	25.77	48.99
ALS/UltraCam	MLR	0.35	−4.38	24.62	46.80
	k-NN	0.34	−3.65	24.86	47.26
	SVR	0.39	−5.88	23.93	45.49
	RF	0.31	−2.13	25.39	48.27
PALSAR/UltraCam	MLR	0.23	−6.23	26.93	51.18
	k-NN	0.20	−1.26	27.54	52.35
	SVR	0.20	2.57	27.50	52.27
	RF	0.21	−0.22	27.27	51.83
ALS/PALSAR/UltraCam	MLR	0.28	−6.26	25.94	49.31
	k-NN	0.38	−3.76	24.20	46.00
	SVR	0.35	−6.96	24.73	47.01
	RF	0.32	−1.94	25.33	48.14

3.2. AFCS estimation

Estimates of mean AFCS and the corresponding SEs obtained using the most accurate algorithm for each remotely sensed dataset separately are presented in Table 4. The pure field-based estimate of the mean AFCS was 52.61 Mg ha^{-1} with SE = 3.05 Mg ha^{-1}. For the model-assisted estimators, estimates of mean AFCS ranged from 51.47 Mg ha^{-1} for ALS to 55.39 Mg ha^{-1} for the ALS, PALSAR and UltraCam combination. The model-assisted estimates were within an approximate 95% confidence interval for the pure field-based estimate (46.57–59.16 Mg ha^{-1}). The estimate of the population mean based on ALS and PALSAR combination was closest to the field-based estimate and had the greatest explanatory power with R^{2*} = 0.41. SEs obtained using the various remotely sensed datasets ranged from 2.34 Mg ha^{-1} for the ALS and PALSAR combination to 2.97 Mg ha^{-1} for PALSAR. Also, RE ranged between 1.05 for PALSAR and 1.70 for the ALS and PALSAR combination. The smallest SE and the largest RE were obtained for the ALS and PALSAR combination which had greater accuracy than the other datasets. Of importance, RE = 1.70 for the ALS and PALSAR combination indicates that the sample size would have to be increased by 70% to achieve the same precision without use of the remotely sensed data as was achieved with it. Sample size increases of 70% are substantial and in many cases may be prohibitive. Graphs of observed versus predicted AFCS for each of the seven remotely sensed datasets are presented in Fig. 2.

Table 4
Estimates of the mean ($\hat{\mu}_{MA}$) standard error (SE ($\hat{\mu}_{MA}$) and relative efficiency (RE) for the seven remotely sensed datasets.

Dataset	$\hat{\mu}_{MA}$ (Mg ha^{-1})	SE ($\hat{\mu}_{MA}$) (Mg ha^{-1})	RE
ALS	51.47	2.48	1.51
PALSAR	52.67	2.97	1.05
UltraCam	53.51	2.66	1.32
ALS/PALSAR	52.64	2.34	1.70
ALS/UltraCam	54.79	2.38	1.65
PALSAR/UltraCam	53.72	2.71	1.27
ALS/PALSAR/UltraCam	55.39	2.40	1.61

4. Summary

Mutiple studies focusing on the utility of combining remotely sensed data from multiple sources for AGB/AFCS estimation have been reported (Montesano et al., 2013; Chopping et al., 2011; Sun et al., 2011). The ability of ALS data to predict forest structural variables makes it a powerful data source for forest AGB/AFCS prediction, even though its point intensity is from only a single wavelength. However, the tradeoffs among plot size, costs and the precision of ALS-assisted AGB/AFCS estimates need to be evaluated for different forest types. Conversely, optical data provide a greater range of spectral information but are mostly unable to predict forest structure. Thus, ALS and optical data can be complementary as we found, although, some studies have reported no or only slight improvement in AGB prediction resulting from the synergy of ALS and optical data (Latifi et al., 2012; Clark et al., 2011). The ability of SAR data to penetrate forest canopies relative to optical sensors contribute to its potential to produce positive effects when used in combination with data from other sensors (Slatton et al., 2002; Moghaddam et al., 2002). For this study, however, integration of PALSAR data with UltraCam data yielded no improvement in AFCS estimates and actually produced smaller R^{2*}. This result can be at least partially attributed to our biophysically complex site, the accuracy of DEM for geocoding, and the exclusion of trees with dbh < 12.5 cm even though they were subject to SAR backscattering (Robinson et al., 2013). Instead, as we expected, the greatest accuracy was achieved by integrating ALS with PALSAR data. This result can be attributed to several aspects of measurement physics and sensitivity of lidar and SAR data to different forest structures, thereby contributing to their potential to produce positive effects when used in combination (Tsui et al., 2012; Saatchi, 2010).

The relationships between AGB/AFCS and remote sensing-based metrics are often so complex that formulating the explicit structural models required for parametric algorithms may be very difficult. In our study, the nonparametric prediction techniques with their data-driven model structures were more accurate for AFCS prediction than the parametric MLR for five of seven datasets. When combining remotely sensed datasets for AGB/AFCS prediction, the selected algorithm should be able to accommodate the different characteristics of multisource data (Lu et al., 2014). As with much of the reported literature (Vafaei et al., 2018; García-Gutiérrez et al., 2015; Latifi et al., 2010; Goetz et al., 2009), we used comparative analyses to select the most accurate prediction techniques. In our case, the relatively small differences among prediction techniques can be attributed to minor difference in these techniques.

Multiple factors not explicitly investigated for this study could have affected the results. Firstly, for prediction techniques such as k-NN, inclusion of irrelevant predictor variables can have detrimental effects. Thus, selection of appropriate predictor variables is important for effective AGB/AFCS prediction, particularly when the variables represent different sensors. Secondly, many authors have suggested that the relative errors of AGB/AFCS prediction can vary from 5% to 30% depending on the forest ecosystem, topography, remotely sensed data, forest measurements, and statistical estimators (Chen et al., 2016; Mascaro et al., 2011; Nabuurs et al., 2008; Saatchi et al., 2007; Chen et al., 2000). Thus, uncertainty analyses are required before formulating any definitive conclusions regarding the potential of remotely sensed datasets for predicting AFCS. Although we followed the customary practice of ignoring allometric model prediction uncertainty, some adverse effects were likely, particularly for rare species for which species-specific models are not available. This topic is of increasing recent interest and merits additional attention for all AGB estimation studies (McRoberts et al., 2016). Finally, statistically rigorous designs and corresponding prediction methods, as opposed to ad hoc methods with unknown properties, are required to produce greater efficiency in MRV systems (Gregoire et al., 2016). Based on these factors, generalizations of the results of this study should be made with caution.

5. Conclusions

We evaluated the potential of ALS, PALSAR, and UltraCam remotely sensed datasets, singly and in combination, for AFCS prediction using a variety of techniques. Three main conclusions can be drawn from this study. Firstly, the ALS data had greater potential than the other remotely sensed datasets for improving prediction of AFCS with R^{2*} = 0.34, rRMSE = 47.42% and estimation of mean AFCS with RE = 1.51. Secondly, as expected, the combination of ALS and PALSAR dataset increased RE by 0.18 relative to ALS alone and by 0.64 relative to PALSAR alone. Thirdly, the nonparametric algorithms were more accurate than the MLR prediction technique. These conclusions are specific to this study, although we note that science generally advances via the accumulation and generalization of the results for such individual studies.

Credit authorship contribution statement

Maryam Poorazimy: Conceptualization, Methodology, Data curation, Validation, Formal analysis, Investigation, Writing - original draft, Writing - review & editing, Visualization. **Shaban Shataee:** Conceptualization, Methodology, Resources, Supervision. **Ronald E. McRoberts:** Conceptualization, Methodology, Writing - review & editing. **Jahangir Mohammadi:** Formal analysis, Data curation, Resources.

Declaration of competing interest

The authors declare that they have no known competing financial interests or personal relationships that could have appeared to influence the work reported in this paper.

References

Amini, J., Sadeghi, J., 2011. Optical and radar images in northern forests of Iran biomass estimation. Iranian remote sensing and GIS. 4 (4), 69–82.
Anderson, J.E., Plourde, L.C., Martin, M.E., Braswell, B.H., Smith, M.L., Dubayah, R.O., Hofton, M.A., Blair, J.B., 2008. Integrating waveform LiDAR with hyperspectral imagery for inventory of a northern temperate forest. Remote Sens. Environ. 112, 1856–1870.
Asner, G.P., Mascaro, J., 2014. Mapping tropical forest carbon: calibrating plot estimates to a simple LiDAR metric. Remote Sens. Environ. 140, 614–624.
Attarchi, S., Gloaguen, R., 2014. Improving the estimation of above ground biomass using dual polarimetric PALSAR and ETM+ data in the Hyrcanian Mountain Forest (Iran). Remote Sens. 6, 3693–3715.
Austin, J.M., Mackey, B.G., Van Niel, K.P., 2003. Estimating forest biomass using satellite radar: an exploratory study in a temperate Australian Eucalyptus forest. For. Ecol. Manag. 176, 575–583.
Baskerville, G.L., 1971. Use of logarithmic regression in the estimation of plant biomass. Can. J. For. Res. 2, 49–53.
Belsley, D., Kuh, E., Welsch, R., 1980. Regression Diagnostics: Identifying Influential Data and Sources of Collinearity, illustrated edition. John Wiley & Sons, New York.
Birth, G.S., Mcvey, G.R., 1968. Measuring the color of growing turf with a reflectance spectrophotometer. Agron. J. 60, 640–643.
Breiman, L., 2001. Random forests. Mach. Learn. 45 (1), 5–32.
Brown, S., Gillespie, A.J.R., Lugo, A.E., 1989. Biomass estimation methods for tropical forests with applications to forest inventory data. For. Sci. 35, 881–902.
Buschmann, C., Nagel, E., 1993. In vivo spectroscopy and internal optics of leaves as basis for remote sensing of vegetation. Int. J. Remote Sens. 14 (4), 711–722.
Carreiras, J.M.B., Vasconcelos, M.J., Lucas, R.M., 2012. Understanding the relationship between aboveground biomass and ALOS PALSAR data in the forests of Guinea-Bissau (West Africa). Remote Sens. Environ. 121, 426–442.
Castel, T., Beaudoin, A., Stach, N., Stussi, N., Toan, T.L., Durand, P., 2001. Sensitivity of space-borne SAR data to forest parameters over sloping terrain. Theory and experiment. Int. J. Remote Sens. 22 (12), 2351–2376.
Chen, Q., McRoberts, R.E., Wang, C., J. Radtke, P., 2016. Forest aboveground biomass mapping and estimation across multiple spatial scales using model-based inference. Remote Sens. Environ. 184, 350–360.
Chen, W., Chen, J., Liu, J., Cihlar, J., 2000. Approaches for reducing uncertainties in regional forest carbon balance. Glob. Biogeochem. Cycles. 14, 827–838.
Chirici, G., Mura, M., McInerney, D., Py, N., Tomppo, E.O., Waser, L.T., Travaglini, D., McRoberts, R.E., 2016. A meta-analysis and review of the literature on the k-nearest neighbors technique for forestry applications that use remotely sensed data. Remote Sens. Environ. 176, 282–294.
Chopping, M., Schaaf, C.B., Zhao, F., Wang, Z., Nolin, A.W., Moisen, G.G., Martonchik,

J.V., Bull, M., 2011. Forest structure and aboveground biomass in the southwestern United States from MODIS and MISR. Remote Sens. Environ. 115, 2943–2953.
Clark, M.L., Roberts, D.A., Ewel, J.J., Clark, D.B., 2011. Estimation of tropical rain forest aboveground biomass with small-footprint lidar and hyperspectral sensors. Remote Sens. Environ. 115, 2931–2942.
Cloude, S.R., Pottier, E., 1997. An entropy based classification scheme for land applications of polarimetric SAR. IEEE Trans. Geosci. Remote Sens. 35 (1), 68–78.
Deng, S., Katoh, M., Guan, Q., Yin, N., Li, M., 2014. Estimating forest aboveground biomass by combining ALOS PALSAR and WorldView-2 data: a case study at Purple Mountain National Park, Nanjing, China. Remote Sens. 6 (9), 7878–7910.
Dobson, M.C., Ulaby, F.T., LeToan, T., Beaudoin, A., Kasischke, E.S., Christensen, N., 1992. Dependence of radar backscatter on coniferous forest biomass. IEEE Trans. Geosci. Remote Sens. 30 (2), 412–415.
Fathollahi, M., 2013. Investigation of Aboveground Carbon Stock Estimation Using SPOT-HRG Data (Case Study: Darab Kolah Forest). A Thesis of Master Student. Sari university of Agriculture and Natural Resources (68p).
Fernández-Manso, O., Fernández-Manso, A., Quintano, C., 2014. Estimation of aboveground biomass in Mediterranean forests by statistical modelling of ASTER fraction images. Int. J. Appl. Earth Obs. Geoinf. 31, 45–56.
Galeaña-Pizaña, J.M., López-Caloca, A., López-Quiroz, P., Silván-Cárdenasa, J.L., Couturier, S., 2014. Modeling the spatial distribution of aboveground carbon in Mexican coniferous forests using remote sensing and a geostatistical approach. Int. J. Appl. Earth Obs. Geoinf. 30, 179–189.
García, M., Riaño, D., Chuvieco, E., Danson, F.M., 2010. Estimating biomass carbon stocks for a Mediterranean forest in central Spain using LiDAR height and intensity data. Remote Sens. Environ. 114, 816–830.
García-Gutiérrez, J., Martínez-Álvarez, F., Troncoso, A., Riquelme, J.C., 2015. A comparison of machine learning regression techniques for LiDAR-derived estimation of forest variables. Neurocomputing 167, 24–31.
Gibbs, H.K., Brown, S., Niles, J.O., Foley, J.A., 2007. Monitoring and estimating tropical forest carbon stocks: making REDD a reality. Environ. Res. Lett. 2 (4), 045023.
Gjertsen, A.K., 2007. Accuracy of forest mapping based on Landsat TM data and a k-NN-based method. Remote Sens. Environ. 110, 420–430.
Gleason, C., Im, J., 2012. Forest biomass estimation from airborne LiDAR data using machine learning approaches. Remote Sens. Environ. 125, 80–91.
Global Forest Observations Initiative (GFOI), 2016. Integration of remote-sensing and ground-based observations for estimation of emissions and removals of greenhouse gases in forests. In: Methods and Guidance from the Global Forest Observations Initiative, Edition 2.0. UN Food and Agriculture Organization (224p).
Goetz, S., Baccini, A., Laporte, N., Johns, T., Walker, W., Kellndorfer, J., Houghton, R., Sun, M., 2009. Mapping and monitoring carbon stocks with satellite observations: a comparison of methods. Carbon Balance Manag. 4 (2), 1–7.
Gregoire, T.G., Næsset, E., McRoberts, R.E., Ståhl, G., Andersen, H.E., Gobakken, T., Ene, L., Nelson, R., 2016. Statistical rigor in LiDAR-assisted estimation of aboveground forest biomass. Remote Sens. Environ. 173, 98–108.
Hamdan, O., Mohd Hasmadi, I., Khali Aziz1, H., Norizah, K., Helmi Zulhaidi, M., 2015. L-band saturation level for aboveground biomass of dipterocarp forests in peninsular Malaysia. J. Trop. For. Sci. 27 (3), 388–399.
Haralick, R.M., Shanmugam, K., Dinstein, I., 1973. Textural features for image classification. IEEE Trans. Syst. Man Cybern. 3 (6), 610–621.
Hopkinson, C., Chasmer, L., Barr, A.G., Kljun, N., Black, T.A., McCaughey, J.H., 2016. Monitoring boreal forest biomass and carbon storage change by integrating airborne laser scanning, biometry and eddy covariance data. Remote Sens. Environ. 181, 82–95.
Houghton, R.A., 2005. Aboveground forest biomass and the global carbon balance. Glob. Chang. Biol. 11, 945–958.
Hudak, A.T., Strand, E.K., Vierling, L.A., Byrne, J.C., Eitel, J.U.H., Martinuzzi, S., Falkowski, M.J., 2012. Quantifying aboveground forest carbon pools and fluxes from repeat LiDAR surveys. Remote Sens. Environ. 123, 25–40.
Huete, A.R., 1988. A soil-adjusted vegetation index (SAVI). Remote Sens. Environ. 25, 295–309.
Imhoff, M.L., 1995. Radar backscatter and biomass saturation: ramifications for global biomass inventory. IEEE Trans. Geosci. Remote Sens. 33 (2), 511–518.
IPCC, 2006. In: Eggleston, H.S., Buendia, L., Miwa, K., Ngara, T., Tanabe, K. (Eds.), IPCC Guidelines for National Greenhouse gas Inventories, Volume 4 (Agriculture, Forestry and Other Land Use), National Greenhouse Gas Inventories Program. IGES, Hayama Available at. http://www.ipcc-nggip.iges.or.jp/public/2006gl/vol4.html.
Jinwei, D., Xiangming, X., Sage, S., Chandrashekar, B., Guishui, X., 2012. Mapping tropical forests and rubber plantations in complex landscapes by integrating PALSAR and MODIS imagery. ISPRS J. Photogramm. Remote Sens. 74, 20–33.
Kachamba, D., Ørka, H., Gobakken, T., Eid, T., Mwase, W., 2016. Biomass estimation using 3D data from unmanned aerial vehicle imagery in a tropical woodland. Remote Sens. 8 (11), 968.
Kaufman, Y.J., Tanre, D., 1992. Atmospherically resistant vegetation index (ARVI) for EOS-MODIS. IEEE Trans. Geoscience and Remote Sensing. 30, 261–270.
Kellndorfer, J.M., Pierce, L.E., Dobson, M.C., Ulaby, F.T., 1998. Toward consistent regional-to-global-scale vegetation characterization using orbital SAR systems. IEEE Trans. Geosci. Remote Sens. 36 (5), 1396–1411.
Kim, C., 2012. Quantitative analysis of relationship between ALOS PALSAR backscatter and forest stand volume. J. Mar. Sci. Technol. 20, 624–628.
Koch, B., 2010. Status and future of laser scanning, synthetic aperture radar and hyperspectral remote sensing data for forest biomass assessment. ISPRS J. Photogramm. Remote Sens. 65, 581–590.
Kraus, K., Pfeifer, N., 1998. Determination of terrain models in wooded areas with airborne laser scanner data. ISPRS J. Photogrammetry remote sensing. 53, 193–203.
Kronseder, K., Ballhorn, U., Bhm, V., Siegert, F., 2012. Above ground biomass estimation across forest types at different degradation levels in central Kalimantan using LiDAR data. Int. J. Appl. Earth Obs. Geoinf. 18, 37–48.
Latifi, H., Nothdurft, A., Koch, B., 2010. Nonparametric prediction and mapping of standing timber volume and biomass in a temperate forest: application of multiple optical/LiDAR-derived predictors. Forestry. 83, 395–407.
Latifi, H., Fassnacht, F., Koch, B., 2012. Forest structure modeling with combined airborne hyperspectral and LiDAR data. Remote Sens. Environ. 121, 10–25.
Le Toan, T., Quegan, S., Woodward, I., Lomas, M., Delbart, N., Picard, G., 2004. Relating radar remote sensing of biomass to modelling of forest carbon budgets. Clim. Chang. 67, 379–402.
Lee, J.S., 1981. Refined filtering of image noise using local statistics. Comput. Graphics Image Process. 15, 380–389.
Lim, K.S., Treitz, P.M., 2004. Estimation of above ground forest biomass from airborne discrete return laser scanner data using canopy-based quantile estimators. Scand. J. For. Res. 19, 558–570.
Lu, D., 2006. A review-the potential and challenge of remote sensing-based biomass estimation. Int. J. Remote Sens. 27 (7), 1297–1328.
Lu, D., Mausel, P., Brondizio, E., Moran, E., 2004. Relationship between forest stand parameters and Landsat TM spectral response in the Brazilian Amazon Basin. For. Ecol. Manag. 198 (1–3), 149–167.
Lu, D., Chen, Q., Wang, G., Liu, L., Li, G., Moran, E., 2014. A survey of remote sensing-based aboveground biomass estimation methods in forest ecosystems. Int. J. Digital Earth. 9 (1), 63–105.
Lucas, R., Armston, J., Fairfax, R., Fensham, R., Accad, A., Carreiras, J., Kelley, J., Bunting, P., Clewley, D., Bray, S., Metcalfe, D., 2010. An evaluation of the ALOS PALSAR L-band backscatter—Above ground biomass relationship Queensland, Australia: Impacts of surface moisture condition and vegetation structure. IEEE Journal of Selected Topics in Applied Earth Observations and Remote Sensing. 3 (4): 576-593.
Luckman, A., Baker, J., Kuplich, T.M., Yanasse, C.D.F., Frery, A.C., 1997. A study of the relationship between radar backscatter and regenerating tropical forest biomass for spaceborne SAR instruments. Remote Sens. Environ. 60, 1–13.
Marabel, M., Alvarez-Taboada, F., 2013. Spectroscopic determination of aboveground biomass in grasslands using spectral transformations, support vector machine and partial least squares regression. Sensors 13, 10027–10051.
Mascaro, J., Detto, M., Asner, G.P., Muller-Landau, H.C., 2011. Evaluating uncertainty in mapping forest carbon with airborne LiDAR. Remote Sens. Environ. 115, 3770–3774.
Mathieu, R., Pouget, M., Cervelle, B., Escadafal, R., 1998. Relationships between satellite-based radiometric indices simulated using laboratory reflectance data and typic soil color of an arid environment. Remote Sens. Environ. 66, 17–28.
Mauya, E.W., Hansen, E.H., Gobakken, T., Bollandsås, O., Malimbwi, R.E., Næsset, E., 2015. Effects of field plot size on prediction accuracy of aboveground biomass in airborne laser scanning-assisted inventories in tropical rain forests of Tanzania. Carbon Balance Manag. 10 (1), 10.
McGaughey, R.J., 2015. FUSION/LDV: Software for LiDAR Data Analysis and Visualization, Version 3.50, First edition. United State Department of Agriculture (USDA), Forest Service Pacific Northwest Research Station, Washington, DC.
McRoberts, R.E., 2012. Estimating forest attribute parameters for small areas using nearest neighbors techniques. For. Ecol. Manag. 272, 3–12.
McRoberts, R.E., Næsset, E., Gobakken, T., 2015. Optimizing the k-nearest neighbors technique for estimating forest aboveground biomass using airborne laser scanning data. Remote Sens. Environ. 163, 13–22.
McRoberts, R.E., Chen, Q., Domke, G.W., Ståhl, G., Saarela, S., Westfall, J.A., 2016. Hybrid estimators for mean aboveground carbon per unit area. For. Ecol. Manag. 378, 44–56.
Means, J.E., Acker, S.A., Harding, D.J., Blair, J.B., Lefsky, M.A., Cohen, W.B., Harmon, M.E., McKee, W.A., 1999. Use of large-footprint scanning airborne lidar to estimate forest stand characteristics in the Western Cascades of Oregon. Remote Sens. Environ. 67 (3), 298–308.
Miettinen, J., Liew, S.C., 2011. Separability of insular Southeast Asian woody plantation species in the 50 m resolution ALOS PALSAR mosaic product. IEEE Geosci. Remote Sens. Lett. 2 (4), 299–307.
Mitchard, E., Saatchi, S., Woodhouse, I., Nangendo, G., Ribeiro, N., Williams, M., 2009. Using satellite radar backscatter to predict above-ground woody biomass: A consistent relationship across four different African landscapes. Geophys. Res. Lett. 36, L23401.
Moghaddam, M., Dungan, J.L., Acker, S., 2002. Forest variable estimation from fusion of SAR and multispectral optical data. IEEE Trans. Geosci. Remote Sens. 40 (10), 2176–2187.
Mohammadi, J., 2013. Improving in Estimation of Some Forest Structure Quantitative Characteristics by Combining the Lidar and Digital Aerial Images in Shast Kalate Hardwood Forests of Gorgan. A thesis of PhD student. Gorgan University of agriculture Science and natural resources (287p).
Montesano, P.M., Cook, B.D., Sun, G., Simard, M., Nelson, R.F., Ranson, K.J., Zhang, Z., Luthcke, S., 2013. Achieving accuracy requirements for forest biomass mapping: a spaceborne data fusion method for estimating forest biomass and LiDAR sampling error. Remote Sens. Environ. 130, 153–170.
Mosavi, B., 2015. Comparison of High Resolution (Quickbird) and Medium Resolution (Landsat8-OLI) Satellite Images Capability in Estimation of Trees Aboveground Biomass. A Thesis of Master Student. Gorgan University of Agriculture Science and Natural Resources (132p).
Nabuurs, G.J., van Putten, B., Knippers, T.S., Mohren, G.M.J., 2008. Comparison of uncertainties in carbon sequestration estimates for a tropical and a temperate forest. For. Ecol. Manag. 256, 237–245.
Næsset, E., 2004. Accuracy of forest inventory using airborne laser scaning: evaluating the first Nordic full-scale operational project. Scand. J. For. Res. 19 (6), 554–557.

Næsset, E., Ørka, H.O., Solberg, S., Bollandsås, O.M., Hansen, E.H., Mauya, E., Zahabu, E., Malimbwi, R., Chamuya, N., Olsson, H., Gobakken, T., 2016. Mapping and estimating forest area and aboveground biomass in miombo woodlands in Tanzania using data from airborne laser scanning, TanDEM-X, RapidEye, and global forest maps: A comparison of estimated precision. Remote Sens. Environ. 175, 282–300.
Omar, H., Misman, M., Kassim, A., 2017. Synergetic of PALSAR-2 and Sentinel-1A SAR polarimetry for retrieving aboveground biomass in dipterocarp forest of Malaysia. Appl. Sci. 7 (7), 675.
Patenaude, G., Hill, R.A., Milne, R., Gaveau, D.L.A., Briggs, B.B.J., Dawson, T.P., 2004. Quantifying forest above ground carbon content using LiDAR remote sensing. Remote Sens. Environ. 93, 368–380.
Pereira, L., Furtado, L., Novo, E., Sant'Anna, S., Liesenberg, V., Silva, T., 2018. Multifrequency and full-polarimetric SAR assessment for estimating above ground biomass and leaf area index in the Amazon Várzea wetlands. Remote Sens. 10 (9), 1355.
Pham, T.D., Yoshino, K., Le, N.N., Bui, D.T., 2018. Estimating aboveground biomass of a mangrove plantation on the northern coast of Vietnam using machine learning techniques with an integration of ALOS-2 PALSAR-2 and Sentinel-2A data. Int. J. Remote Sens. 39 (22), 7761–7788.
Powell, S.L., Cohen, W.B., Healey, S.P., Kennedy, R.E., Moisen, G.G., Pierce, K.B., 2010. Quantification of live aboveground forest biomass dynamics with Landsat time-series and field inventory data: a comparison of empirical modeling approaches. Remote Sens. Environ. 114, 1053–1068.
Robinson, C., Saatchi, S., Neumann, M., Gillespie, T., 2013. Impacts of spatial variability on aboveground biomass estimation from L-band radar in a temperate forest. Remote Sens. 5, 1001–1023.
Ronoud, Q., 2016. Estimating Aboveground Woody Biomass of Fagus Orientalis Stands in Hyrcanian Forest of Iran Using Landsat 8 Satellite Data (Case Study: Khyroud Forest). A Thesis of Master Student. University of Tehran (103p).
Roujean, J.L., Breon, F.M., 1995. Estimating PAR absorbed by vegetation from bidirectional reflectance measurements. Remote Sens. Environ. 51, 375–384.
Rouse, J.W., Haas, R.H., Schell, J.A., Deering, D.W., 1973. Monitoring vegetation systems in the Great Plains with ERTS. In: Third Earth Resources Technology Satellite-1 Symposium, 10–14 December, Washington, DC. NASA, Washington, DC, pp. 309–317.
Saatchi, S., 2010. Synergism of optical and radar data for forest structure and biomass Sinergismo entre dados ópticos e de radar da estrutura da floresta e biomassa. Ambiência 6 (4), 151–166.
Saatchi, S., Houghton, R.A., Alvalá, R.C., Soares, J.V., Yu, Y., 2007. Distribution of aboveground live biomass in the Amazon basin. Glob. Chang. Biol. 13, 816–837.
Saatchi, S., Marlier, M., Chazdon, R.L., Clark, D.B., Russell, A.E., 2011. Impact of spatial variability of tropical forest structure on radar estimation of aboveground biomass. Remote Sens. Environ. 115 (11), 2836–2849.
Sagheb-Talebi, k, Pourhashemi, M., Sajedi, T., 2014. Forests of Iran: A Treasure From the Past, a Hope for the Future, First edition. Springer Science and Business Media, New York.
Santoro, M., Eriksson, L., Askne, J., Schmullius, C., 2006. Assessments of stand-wise stem volume retrieval in boreal forest from JERS-1 L-band SAR backscatter. Int. J. Remote Sens. 27 (16), 3425–3454.
Santoro, M., Fransson, J.E., Eriksson, L.E., Magnusson, M., Ulander, L.M., Olsson, H., 2009. Signatures of ALOS PALSAR L-band backscatter in Swedish forest. IEEE Trans. Geosci. Remote Sens. 47, 4001–4019.
Särndal, C.-E., Swensson, B., Wretman, J., 1992. Model Assisted Survey Sampling. Springer, New York.
Shamsi Jamkhaneh, S., 2012. Estimation of Tree Biomass Using Some Environmental Factors by Emphasize on Soil Characteristics. A thesis of Master Student. Gorgan university of Agriculture Science and Natural Resources (166p).
Shimada, M., Isoguchi, O., Tadono, T., Isono, K., 2009. Palsar radiometric and geo-metric calibration. IEEE Trans. Geosci. Remote Sens. 47 (12), 3915–3932.
Sinha, S., Jeganathan, C., Sharma, L.K., Nathawat, M.S., 2015. A review of radar remote sensing for biomass estimation. Int. J. Environ. Sci. Technol. 12, 1779–1792.
Slatton, K.C., Crawford, M.M., Evans, B.L., 2002. Fusing interferometric radar and laser altimeter data to estimate surface topography and vegetation heights. IEEE Trans. Geosci. Remote Sens. 39 (11), 2470–2482.
Ståhl, G., Saarela, S., Schnell, S., Holm, S., Breidenbach, J., Healey, S.P., Patterson, P.L., Magnussen, S., Næsset, E., McRoberts, R.E., Gregoire, T.G., 2016. Use of models in large-area forest surveys: comparing model-assisted, model-based and hybrid estimation. Forest Ecosystems. 3 (1): 5.
Stelmaszczuk-Górska, M., Urbazaev, M., Schmullius, C., Thiel, C., 2018. Estimation of above-ground biomass over boreal forests in Siberia using updated in situ, ALOS-2 PALSAR-2, and RADARSAT-2 data. Remote Sens. 10 (10), 1550.
Sun, G., Ranson, K.J., Guo, Z., Zhang, Z., Montesano, P., Kimes, D., 2011. Forest biomass mapping from lidar and radar synergies. Remote Sens. Environ. 115, 2906–2916.
Suzuki, R., Kim, Y., Ishii, R., 2013. Sensitivity of the backscatter intensity of ALOS/PALSAR to the above-ground biomass and other biophysical parameters of boreal forest in Alaska. Polar Sci. 7, 100–112.
Tanase, M.A., Panciera, R., Lowell, K., Tian, S., Hacker, J.M., Walker, J.P., 2014. Airborne multi-temporal L-band polarimetric SAR data for biomass estimation in semi-arid forests. Remote Sens. Environ. 145, 93–104.
Thapa, R.B., Watanabe, M., Motohka, T., Shimada, M., 2015. Potential of high-resolution ALOS–PALSAR mosaic texture for aboveground forest carbon tracking in tropical region. Remote Sens. Environ. 160, 122–133.
Thiel, C.J., Thiel, C., Schmullius, C.C., 2009. Operational large-area forest monitoring in Siberia using ALOS PALSAR summer intensities and winter coherence. IEEE Trans. Geosci. Remote Sens. 47, 3993–4000.
Tian, X., Su, Z., Chen, E., Li, Z., Vander Tol, C., Guo, J., He, Q., 2012. Estimation of forest aboveground biomass using multi-parameter remote sensing data over a cold and arid area. Int. J. Appl. Earth Obs. Geoinf. 17, 102–110.
Tomppo, E., Olsson, H., Ståhl, G., Nilsson, M., Hagner, O., Katila, M., 2008. Combining national forest inventory field plots and remote sensing data for forest databases. Remote Sens. Environ. 112, 1982–1999.
Tsui, O.W., Coops, N.C., Wulder, M.A., Marshall, P.L., Mc Cardle, A., 2012. Using multi-frequency radar and discrete-return LiDAR measurements to estimate aboveground biomass and biomass components in a coastal temperate forest. ISPRS J. Photogramm. Remote Sens. 69, 121–133.
Tsui, O.W., Coops, N.C., Wulder, M.A., Marshall, P.L., 2013. Integrating airborne LiDAR and space-borne radar via multivariate kriging to estimate above-ground biomass. Remote Sens. Environ. 139, 340–352.
Tucker, C.J., 1979. Red and photographic infrared linear combinations for monitoring vegetation. Remote Sens. Environ. 8, 127–150.
Ulander, L.M.H., 1996. Radiometric slope correction of synthetic-aperture radar images. IEEE Trans. Geosci. Remote Sens. 34 (5) (1115-1112).
Vafaei, S., Soosani, J., Adeli, K., Fadaei, H., Naghavi, H., Pham, T., Tien Bui, D., 2018. Improving accuracy estimation of forest aboveground biomass based on incorporation of ALOS-2 PALSAR-2 and Sentinel-2A imagery and machine learning: a case study of the Hyrcanian forest area (Iran). Remote Sens. 10 (2), 172.
Vaglio Laurin, G., Chen, Q., A Lindsell, J., A.coomes, D., Delfrate, F., Guerriero, L., Pirotti, F., Valentini, R., 2014. Above ground biomass estimation in an African tropical forest with lidar and hyperspectral data. ISPRS J. Photogramm. Remote Sens. 89, 49–58.
Vashum, K.T., Jayakumar, S., 2012. Methods to estimate above-ground biomass and carbon stock in natural forests: a review. Ecosyst Ecogr. 2 (116), 1–7.
Wani, A., Joshi, P., Singh, O., 2015. Estimating biomass and carbon mitigation of temperate coniferous forests using spectral modeling and field inventory data. Eco. Inform. 25, 63–70.
Wu, F., Wang, C., Zhang, H., Zhang, B., Tang, Y.X., 2011. Rice crop monitoring in South China with RADARSAT-2 quad-polarization SAR data. IEEE Trans. Geosci. Remote Sens. 8 (2), 196–200.
Yadav, B.K., Nandy, S., 2015. Mapping aboveground woody biomass using forest inventory, remote sensing and geostatistical techniques. Environ. Monit. Assess. 187 (5), 1–12.
Zald, H.S., Wulder, M.A., White, J.C., Hilker, T., Hermosilla, T., Hobart, G.W., Coops, N.C., 2016. Integrating Landsat pixel composites and change metrics with lidar plots to predictively map forest structure and aboveground biomass in Saskatchewan, Canada. Remote Sens. Environ. 176, 188–201.
Zhao, P., Lu, D., Wang, G., Liu, L., Li, D., Zhu, J., Yu, S., 2016. Forest aboveground biomass estimation in Zhejiang Province usingthe integration of Landsat TM and ALOS PALSAR data. Int. J. Appl. Earth Obs. Geoinf. 53, 1–15.
Zhou, G., Xu, X., Du, H., Ge, H., Shi, Y., Zhou, Y., 2011. Estimating aboveground carbon of Moso bamboo forests using the k nearest neighbors technique and satellite imagery. Photogramm. Eng. Remote. Sens. 77 (11), 1123–1131.
Zolkos, S.G., Goetz, S.J., Dubayah, R., 2013. A meta-analysis of terrestrial aboveground biomass estimation using lidar remote sensing. Remote Sens. Environ. 128, 289–298.